

Anatomically and Dielectrically Realistic Microwave Head Phantom with Circulation and Reconfigurable Lesions

Barry McDermott^{1, *}, Emily Porter¹, Adam Santorelli¹, Brendan Divilly², Liam Morris²,
Marggie Jones¹, Brian McGinley¹, and Martin O'Halloran¹

Abstract—Phantoms provide valuable test platforms for developing medical devices. Solid materials in particular allow fabrication of stable and robust models. This paper presents a novel, anatomically realistic, multi-layered head phantom made from dielectrically accurate, stable, easily mouldable, low-cost tissue-mimicking materials for testing of microwave diagnostic systems. Also incorporated is a mechanism for inserting reconfigurable lesions and a novel circulatory system modelling physiology. Tissue-mimicking materials composed of graphite, carbon black, and polyurethane with small volumes of acetone or isopropanol were fabricated and dielectric properties were measured across the 1–8.5 GHz band. The tissue-mimicking material properties were adjusted until their dielectric properties matched those of reference values for target tissues of interest, thereby emulating: weighted aggregates of head tissues external to the brain, tissues comprising the brain, and blood. 3D printed anatomically realistic head and brain moulds cast the phantom mixtures for each layer. Cylindrical holes in the brain layer allow insertion of pathological lesion phantoms, such as haemorrhages. Tubing embedded in the brain layer forms a symmetrical loop providing a novel simplistic model of circulation. The resulting head phantom is anatomically realistic, dielectrically stable, enables pathology modelling, and has, uniquely, a circulatory loop. This novel head phantom provides a valuable test platform for microwave diagnostic studies.

1. INTRODUCTION

Many significant pathologies with structural aetiologies affect the brain. These include haemorrhagic brain diseases, for example haemorrhagic stroke and the variety of bleed types caused by traumatic brain injury (TBI) [1, 2]. Other pathologies featuring structural lesions include cancer, where tumours may be present in the brain parenchyma. For many of these conditions, diagnostic imaging forms a crucial step pre-treatment. Gold standard imaging modalities include Computed Tomography (CT) and Magnetic Resonance Imaging (MRI). These technologies offer excellent anatomical detail but are not without their drawbacks, which include cost, radiation exposure in CT, and the strong magnetic fields and bulk of machine associated with MRI, leading to contraindications for patients with pacemakers and those with claustrophobia [3]. Most significantly, there is a lack of access to these imaging modalities due to the high associated costs which limit their availability in smaller or rural facilities, and the requirement for experienced radiologists to assess the results [3], meaning that the technologies are not universally available to patients who need it.

An emerging modality in the field of biomedical imaging is that of microwave diagnostics (MWD), which relies on the contrast in dielectric properties of biological tissues: relative permittivity (ϵ_r) and conductivity (σ) [4]. This technology has the potential to be translated into non-invasive, portable,

Received 18 July 2017, Accepted 9 August 2017, Scheduled 18 August 2017

* Corresponding author: Barry McDermott (b.mcdermott3@nuigalway.ie).

¹ Translational Medical Device Laboratory, National University of Ireland Galway, Ireland. ² Department of Mechanical and Industrial Engineering, Galway-Mayo Institute of Technology, Ireland.

low-cost devices, free from harmful ionising radiation, and could be valuable in the diagnostic pathway of neurological patients. Developing such a technology involves testing of devices using methods that range from computer simulations to trials on animal and human subjects. The former suffers from the difficulty of modelling all the complexity associated with the head and the microwave device. The latter, though near ideal, is slow, costly, involves ethical considerations, and may expose the entire developing system to a potential excess of variables too soon. Hence, system testing with phantoms, physical objects that emulate the properties of human tissues and organs, is a vital step in the technology development process. Experiments with phantoms allow controlled testing to be performed on a physical real world object.

An ideal phantom is easily fabricated, low-cost, anatomically realistic, mechanically and electrically stable, and accurately models the physical phenomena of interest, which in the case of MWD are the dielectric properties of the tissues of interest [5]. Such a phantom also needs to allow modelling of other characteristics of interest. For example, if testing a tumour detection system, then the ability to implant tumour phantoms at known locations within the head phantom would be desirable. The exact requirements of a phantom will depend on the diagnostic technology being investigated, and the desired test scenarios for the technology to face.

To date, most phantoms have modelled important structural features, both in terms of anatomy and tissue properties. In contrast, there has been very few efforts to emulate physiological functionality [6]. Ultimately a phantom would be more realistic and closer to the ideal of a live subject if it incorporated both structural and functional features. An important physiological system in the brain is the circulatory system, with the flow of blood representing a potential noise source to imaging systems like MWD.

Tissue-mimicking materials (TMMs) are used to construct phantoms. There is a close relationship between the dielectric properties of tissues and the water content of the tissue [7], and the dielectric properties are a function of frequency [8]. Further, the properties of a tissue will show a spread of values between individuals and will also depend on other factors such as age [6, 9]. Despite these complexities, TMMs accurately matching the parameters across the frequency range of interest have been developed for a range of tissues. A TMM or TMM set can then be used to fabricate the tissue or organ of interest, resulting in a phantom.

TMMs can be liquids, usually involving emulsions or other dispersive mixtures of water and oils [6]. These allow easy alteration of the dielectric properties by adjusting the water content, but suffer from issues with dehydration, which alters the dielectric properties. Further, liquid TMMs require a container or vessel to hold their shape. A thorough review of liquid and semi-solid TMMs, and the phantoms constructed from them, is given in [6]. At the other extreme are solid TMMs, which may not contain water, and hence dehydration is not an issue. Such TMMs can maintain shape and dielectric properties for long periods. Solid TMMs also allow more accurate anatomical modelling of organs and enable modular fabrication to allow an accurate representation of the interior of the organ of interest to be realised, complete with pathological lesions if desired. Hence, phantoms constructed from solid TMMs have the advantage of being anatomically realistic and stable over time [6].

Despite the obvious advantages of solid TMMs, there are relatively few being used, particularly for head phantoms. A popular solid TMM, ceramic powder, is presented in [10] and [11] in the development of homogenous single layer head phantom. The material provides a wide relative permittivity range but is not lossy, thus requiring the addition of extra conductive materials like carbon powders and resins to attain an appropriate conductivity range [10]. Fabrication difficulty (relative to liquid and other phantom types) and the more expensive materials involved are drawbacks of this material [6]. One of the more advanced head phantoms reported is [12], which features multiple anatomically realistic modules produced using 3D moulds. This head phantom has a solid exterior shell, and the TMMs within are semi-solids based on agar mixtures [12]. However, [13] reports that the outer shell material used in [12] does not have a realistic relative permittivity value for the aggregate outer layers of the head.

In this work, we present easily fabricated, mouldable, low-cost, mechanically and electrically stable solid TMMs made from polyurethane, graphite, and carbon black. These TMMs are based on those proposed previously in [5, 8] for use in breast phantoms. In this study, we develop such TMMs for head tissues. The addition of small volumes of acetone as a thinning agent increases permittivity as reported in [14] and here, for the first time, isopropanol is used and shown to also increase conductivity

to more realistic levels for a given mixture. Various ratios of the ingredients can mimic a range of tissues. In this study, TMMs for three tissue types are developed: a weighted aggregate of the tissues surrounding the brain (skin, skull, meninges, cerebrospinal fluid (CSF)); a weighted aggregate of brain tissues (grey matter, white matter, CSF); and blood to mimic a pathologic haemorrhagic lesion. The dielectric properties of these tissues are obtained from reference sources [15–17], and the TMM mixtures are adjusted to emulate these aggregate values.

We then designed and fabricated a two-layer realistic head phantom using moulds created from anatomically precise 3D print STL (stereolithography) files of the head [18] and brain [19], with the outer aggregate TMM layer surrounding the inner brain mimicking TMM. Cavities were left in the brain layer, which can be filled with any of a range of easily fabricated plugs containing the brain TMM or blood TMM lesions of known size and location. For the first time, we also modelled the circulatory system by embedding a length of narrow tubing into the brain layer. Fluid flow through the loop replicates blood flow for a more physiologically realistic phantom.

The developed head phantom demonstrates a proof-of-concept for an anatomically accurate, dielectrically realistic phantom that is stable long-term. The phantom provides a reconfigurable test platform that can be employed to develop a MWD system for detecting haemorrhagic lesions of various sizes and locations. The principle can be easily extended to other pathologies such as tumours, and can allow for more intricate modelling depending on the needs of a given study.

The next section details the development of the TMM mixtures, while Section 3 outlines the fabrication process of the head phantom. Finally, Section 4 concludes by discussing the significance of the developed phantom.

2. TISSUE-MIMICKING MATERIAL DEVELOPMENT

In this section, we first outline the rationale for selecting the various head-tissue dielectric reference values. Then, we discuss the TMM fabrication and testing. Finally, the results and the error and uncertainty involved in the dielectric properties of the TMMs are examined.

2.1. Dielectric Reference Values

Historically, several studies have been performed to characterise the dielectric properties of the head and brain. Foster et al. characterised grey and white matter individually, then calculated a weighted average based on the relative proportions of each tissue in order to develop an overall profile of the brain [20]. Other works, such as Schmid et al. characterised only one tissue type in a specific location, for example the grey matter of the temporal lobe [21]. Today, foundational studies such as that of Gabriel [15, 16], form the basis for the commonly used dielectric property database provided by The Foundation for Research on Information Technologies (IT²IS) [17].

The IT²IS database provides single relative permittivity and conductivity values at each frequency point, for each tissue type. However, standardising the dielectric properties of biological tissue is not a trivial matter, and this data cannot be used without additional consideration for the many confounders that impact dielectric data of biological tissues (including animal type, heterogeneity, temperature, measurement technique, sample size, measurement accuracy and uncertainty). Gabriel's work involved combining data on various tissue types of different animals from a variety of studies with the selected data biased towards human *in-vivo* data taken near body temperature [15, 16]. However, there is natural heterogeneity in the properties of any given tissue [22], resulting in varying values at different locations and a further variance seen in the biological tissues' properties due to factors such as pathology, changes in the metabolic activity of the tissue, temperature, and age [15, 23, 24]. There is also uncertainty, and hence variance, introduced by the measurement procedure and possible measurement error in the studies used to generate the reference data used [22, 25]. The result of all these factors, especially the natural heterogeneity and measurement procedure [22], is a band of uncertainty around the reference values. For example, Foster's study reported a variability of about 5–10% in both ϵ_r and σ values at 100 MHz when measuring dielectric properties of the brain [20]. A Gabriel study on rat brains of various ages reported variation of 1–10% for brain tissues but up to 25% for skin and skull tissues [25]. A study by Schmid on human brains analysed soon after death reported a variance of about 6% in both ϵ_r

and σ [21]. Hence, the dielectric properties provided by databases such as IT'IS are imperfect, but nonetheless provide a valuable reference source and are used in this study.

In IT'IS, the dielectric properties of the brain as a whole are equivalent to Gabriel's data from the cerebellum [17]. In other words, it is assumed that the cerebellum dielectric properties are representative of those of the brain in its entirety. In this study, we investigate this cerebellum model, along with a second, more refined, model derived from MRI anatomical studies of the brain by Lüders et al. [26]. Lüders' study had a large sample size of 100 volunteers and showed the dominant tissues present in the brain to be grey matter (55%), white matter (27%) and CSF (18%). These proportions were used to generate a more accurate brain model for this study, called the 'Brain Hybrid'. In this model, data from the IT'IS database for grey matter, white matter, and CSF are weighted at 55:27:18, respectively.

The dielectric properties of these two brain models are shown in Fig. 1 to be similar, but not identical, in properties. The variance and imperfection in reference values for dielectric properties is reflected in this observation. The cerebellum can be considered a simplification of the overall brain and would thus be expected to have similar properties to the more refined Brain Hybrid model. However from a gross anatomy point of view, the cerebellum is composed of grey and white matter in the ratio of approximately 84 : 16 [27]. This inconsistency in tissue composition (with a larger proportion of grey matter and no CSF) accounts for the difference from the Brain Hybrid model. However, depending on the nature of a given study, the simplified cerebellar model may be adequate. Therefore, a TMM mixture emulating the brain would be expected to have properties similar to those of the two models.

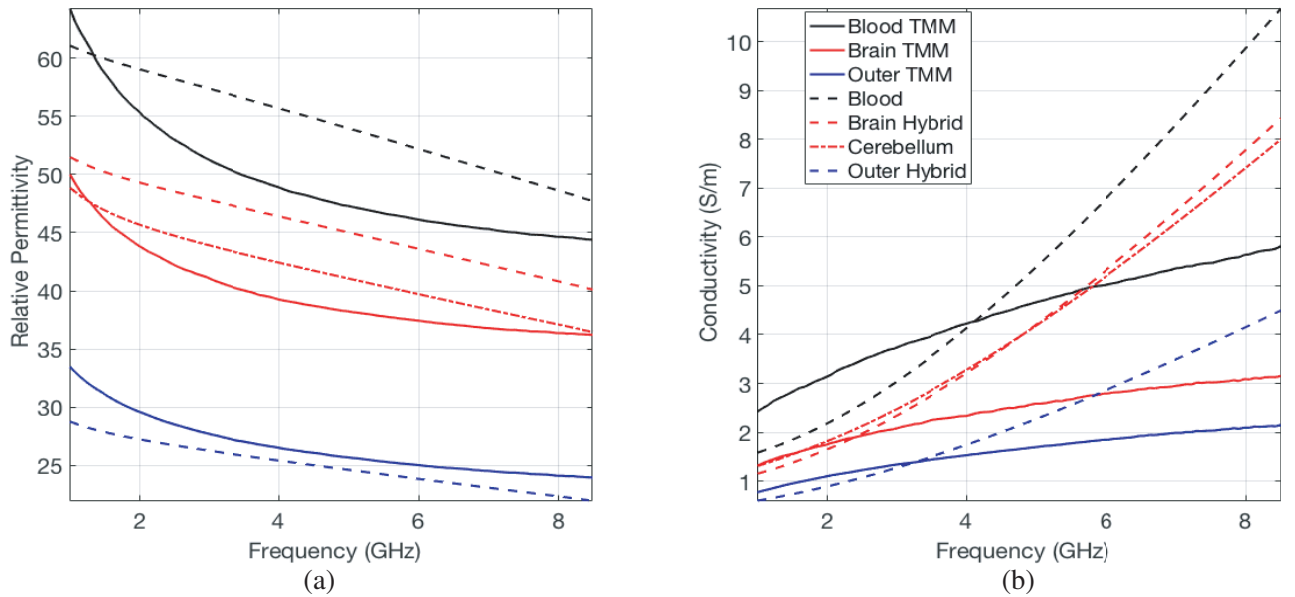


Figure 1. Reference (a) relative permittivity and (b) conductivity curves over the 1–8.5 GHz band for the four tissues of interest: Cerebellum (brain model), Brain Hybrid (refined brain model), Outer Hybrid (model of head tissues external to the brain) and Blood (model). Also shown are the TMM mixtures that most closely mimic each target tissue.

Next, we discuss the tissues of the head exterior to the brain. An approach similar to that taken to produce the Brain Hybrid model was taken to produce a refined estimate of the outer layer of the model. This layer was an aggregate model of skin, skull cortical bone, skull cancellous bone, meninges and subarachnoid CSF (called the 'Outer Hybrid'). The detailed MRI study of Makris et al. is used to calculate the proportions of these tissues as 33%, 34%, 17%, 14% and 2%, respectively [27]. These proportions are used with data from IT'IS to generate the 'Outer Hybrid' dielectric properties profile. Finally, the dielectric properties for blood across the frequency range of 1–8.5 GHz were also referenced from IT'IS. A TMM mimicking blood was used to model haemorrhagic lesions.

Figure 1 shows the relative permittivity and conductivity values for the three tissues across the 1–

8.5 GHz band, as well as those of the TMM mixtures used to mimic them. The TMMs have been developed to match the target values, within the range of inherent biological variability of these parameters. This TMM development and testing is described below in Subsection 2.2.

2.2. Methodology

The presented TMMs are composed of polyurethane, graphite, and carbon black. As described in [5] and [8], polyurethane provides a mechanically strong and flexible base matrix while graphite and carbon black, in varying proportions, can cover most relative permittivity and conductivity ranges seen in biological tissues.

However, high water content tissues, such as blood, which have high relative permittivity and conductivity values, cannot be accurately mimicked using just these components. In [14], it was found that adding small volumes of acetone helped to increase the relative permittivity and conductivity and hence facilitate the replication of high permittivity tissues. Acetone was also proposed to help amalgamate the large amounts of graphite and carbon black involved in such mixtures. Despite adding acetone in similar volumes (typically 0.5–3 ml per 50 g of mixture) to that reported in [14], dielectric values, though increased, were still not high enough to model the high water content tissues of the brain, particularly in terms of conductivity.

In this paper, we propose an alternative solution to increasing the conductivity of the TMMs. In particular, by substituting isopropanol for acetone, the conductivity should be boosted since alcohols are known to hinder agglomeration of graphite and carbon black leading to more conducting pathways [28]. Results, shown in Section 2.3, demonstrate that isopropanol indeed provides the increase in conductivity needed to mimic the tissues adequately. Isopropanol also exhibits similar characteristics to acetone in terms of permittivity and as a mixing aid.

The mixtures described in [14] used to mimic breast tissues were used as a starting point for modification of the mixture ingredient compositions to meet the needs of this study. Sample TMM mixtures were made using the methodology described in [8], each with a different composition of ingredients. These sample mixtures were cast as rectangular cuboids $50 \times 20 \times 20 \text{ mm}^3$. The mixtures were designed to target the three tissues of interest.

The dielectric properties of the sample TMMs were measured across 101 points in a linear sweep over the 1–8.5 GHz band using a Keysight E5063A ENA Series Network Analyser with a performance probe from the Agilent 85070E Dielectric Probe Kit. The dielectric measurement was performed at four random, but not overlapping, points on each sample. The properties measured were the real (ϵ') and imaginary (ϵ'') parts of the complex permittivity. The former is the relative permittivity (ϵ_r) while the latter is related to the conductivity (σ) as shown in (1), where ϵ_0 is the permittivity of free space and f is the frequency in Hz.

$$\sigma = 2\pi f \epsilon_0 \epsilon'' \quad (1)$$

An important consequence of this is that the relative permittivity and conductivity are related and cannot be changed independently of each other.

The measured properties were compared to the target properties for the three tissues of interest. The results were used to design the next set of sample TMMs and this iterative approach followed for 10 iterations until the phantom mixtures created gave converging results as close to the target values as possible, resulting in the final mixtures used to fabricate the head phantom.

2.3. Results & Discussion

The dielectric properties of the final TMM mixtures used to develop the phantom are shown in Fig. 1, which also shows the values of the target tissues. The mean value of four readings at each of 101 measurement points are used to generate the curve for each TMM sample. The makeup of these mixtures is shown in Table 1, with comparisons to reference tissues provided in Tables 2 and 3. We note that there is only one brain TMM, but it is compared to two separate brain models (i.e., the Brain Hybrid and the cerebellum) for completeness, while the other TMM mixtures of the outer layer and blood are compared to a single respective reference value for these tissues.

As can be seen in Fig. 1, the two theoretical models for the aggregate brain tissues closely align but are not identical. The cerebellum model for the brain as a whole is a simplification while the Brain

Table 1. Concentrations, as % w/w (mass percentage), of ingredients used in the final mixtures of each tissue mimicking material.

Target Tissue	Graphite	Carbon Black	Isopropanol	Polyurethane
Blood	44	4	3	49
Brain	44	3	3	50
Outer	30	5.5	0.75	63.75

Table 2. Average percent difference in relative permittivity and conductivity of the TMM mixture and respective reference tissue values across the 1–8.5 GHz band (Note that the reference values themselves show a wide variance as discussed in Section 2.1 above).

Target Tissue	Relative Permittivity (%)	Conductivity (%)	Combined (%)
Blood	10	30	20
Brain Hybrid	13	34	23
Cerebellum	5	33	19
Outer	7	28	17

Table 3. Average percent difference in relative permittivity and conductivity of the TMM mixture and the respective reference tissue values across the 1–4 GHz band (Note that the reference values themselves show a wide variance as discussed in Section 2.1 above).

Target Tissue	Relative Permittivity (%)	Conductivity (%)	Combined (%)
Blood	8	32	12
Brain Hybrid	11	13	12
Cerebellum	5	11	8
Outer	8	16	12

Hybrid model derived from Lüders' MRI study [26] combined with the IT'IS database values [17] is more refined. The percentage difference between the curves for the two models is 8% for relative permittivity, 5% for conductivity giving a combined difference of 6.5%. This result shows the relevance of carefully selecting an appropriate model for biological tissues, as two valid models of an organ can give differing (if similar) results.

From Fig. 1, it is also evident that the mean dielectric properties of the TMMs selected are not a perfect match to the assumed dielectric reference values for the target tissues. This is particularly noticeable in the conductivity plot where it is seen that the shape of the TMM and target tissue curves vary. The permittivity plots are more closely aligned. The objectives of the study were to (1) fit TMMs to within an acceptable error of the reference tissue values and to (2) maintain the contrast between the different tissue types, and these objectives have been achieved.

With regards the first objective, the percent difference between the TMM dielectric properties and those of the target tissues across the 1–8.5 GHz band are shown in Table 2. To calculate these values, the absolute difference between the TMM and the respective reference is calculated at each measurement point. This difference value is divided by the reference value at this point to normalise the difference and is expressed as a percentage. Finally, the mean of these percentage differences across the 101 measurements points is calculated are the final values reported here. Table 3 shows the percent difference across the tighter 1–4 GHz band, where most microwave diagnostic applications exist. The smaller frequency band has lower percent difference values than the wider band. The difference in relative permittivity between a TMM and its respective target tissue is seen to be within the variance

expected in biological tissue of around $\pm 10\%$ [20, 21, 25].

Next, Table 4 displays the standard deviation of the relative permittivity and conductivity measurements from each selected TMM at a representative data point of 4 GHz. The values shown imply that the samples had a good degree of homogeneity, which would be a particular concern with the mixtures containing higher amounts of graphite and carbon black as these were harder to mix.

Table 4. Mean and Standard Deviation of the TMM mixtures for relative permittivity and conductivity at 4 GHz.

TMM Mixture	Relative Permittivity	Conductivity (S/m)
Blood	48.7 ± 2.1	4.2 ± 0.5
Brain	39.3 ± 2.9	2.3 ± 0.5
Outer	26.5 ± 3.0	1.5 ± 0.4

The outcome of second objective, of having the same contrast between the TMMs as exists between the reference tissues, is shown in Table 5. The contrast between each pair of reference tissues is calculated with the contrast between the respective TMM pair shown in italics underneath. These values are calculated for both relative permittivity and conductivity and expressed as a ratio. To calculate this ratio, the value of the relative permittivity or conductivity for the left side member of the pair (as displayed on the table) is set to 1 at each measurement point by self-division with the right side member value adjusted by division with the same value. The mean of these adjusted values across the measurement points gives the final value recorded in the table. As can be seen in Table 5, the contrasts between the TMM pairs are well matched to those of the reference pairs.

Table 5. Contrast ratios between reference tissue pairs and TMM pairs for relative permittivity and conductivity.

Target Tissue Pair Or TMM Mixture Pair	Relative Permittivity (Ratio)	Conductivity (Ratio)
Blood : Brain Hybrid	1 : 0.83	1 : 0.77
Blood : Cerebellum	1 : 0.77	1 : 0.79
<i>Blood TMM : Brain TMM</i>	<i>1 : 0.8</i>	<i>1 : 0.55</i>
Blood : Outer Hybrid	1 : 0.46	1 : 0.41
<i>Blood TMM : Outer TMM</i>	<i>1 : 0.53</i>	<i>1 : 0.36</i>
Brain Hybrid : Outer Hybrid	1 : 0.55	1 : 0.54
Cerebellum : Outer Hybrid	1 : 0.6	1 : 0.53
<i>Brain TMM : Outer TMM</i>	<i>1 : 0.67</i>	<i>1 : 0.65</i>

Lastly, all TMM mixtures were found to be mechanically stable after fabrication. Further, the dielectric properties of the TMMs were re-measured periodically over the course of several weeks with the properties found to be reproducible and not deteriorating by any appreciable amount, similar to the dielectric stability findings in [8].

We note that by varying the amounts of graphite, carbon black, acetone (or isopropanol) and polyurethane, it is possible to cover a broad range of relative permittivity and conductivity profiles which would cover most, if not all, biological tissues. The range covered by the 85 sample phantoms fabricated in this study is shown in Fig. 2. Also shown are reference lines for extremes of biological tissues in terms of relative permittivity and conductivity: blood as a high-water content tissue, and fat, as a low water content tissue.

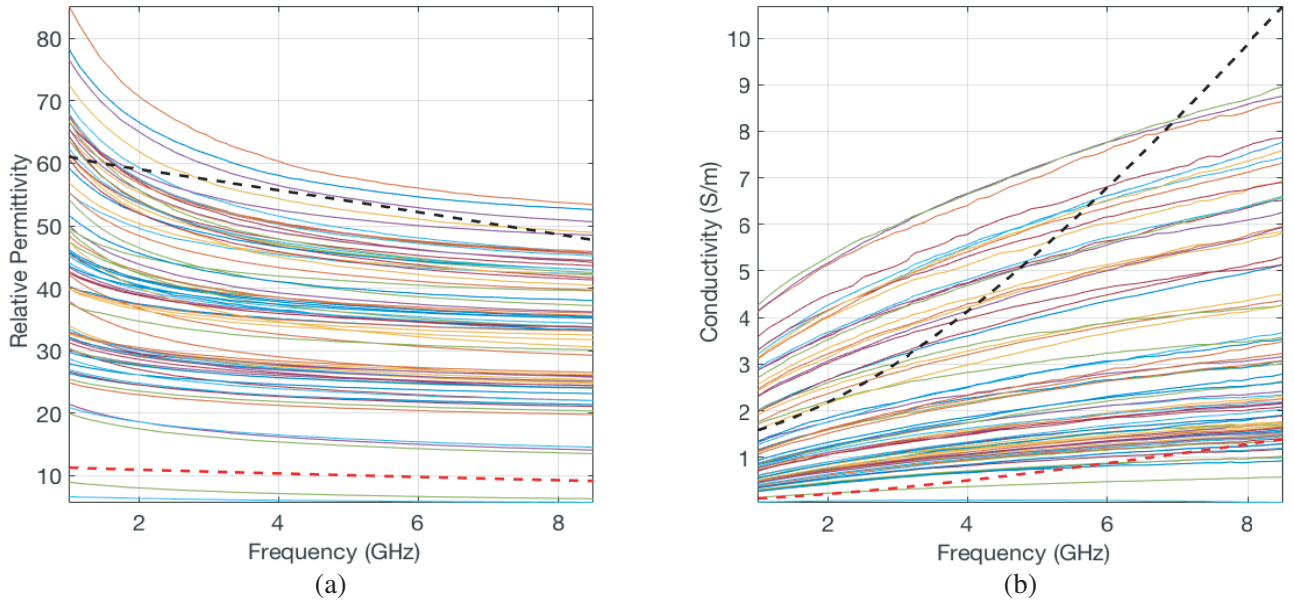


Figure 2. Measured (a) relative permittivity and (b) conductivity curves over the 1–8.5 GHz band for all 85 sample phantom mixtures tested. In dashed lines are the reference values for extreme tissues: blood (black, high water content) and fat (red, very low water content).

3. HEAD PHANTOM FABRICATION

In this section, we present the development of a full head phantom based on the TMMs obtained in Section 2. First, we detail how the head phantom was fabricated and note design choices made along the way. Then, we present the completed head phantom, and discuss its benefits and challenges of fabrication.

3.1. Methodology

The complexity of any phantom fabrication depends on the requisite level of anatomical detail. The degree of accuracy and precision required in replicating an anatomical region of interest will always depend heavily on the needs of a given study. In our work, we have chosen to develop a two-layer phantom, comprising a weighted aggregate layer of tissues external to the brain and an inner weighted aggregate of brain tissues. The phantom has the additional feature of removable and modifiable cylindrical plugs. These plugs can be used to model haemorrhages, based on the developed blood TMM. This phantom composition is clearly a simplification of the true anatomy, for example other head structures such as the nose, eyes and ears are all modelled as the external aggregate tissue while the entire brain is modelled a homogenous mass. However, this structure is more than adequate for early-stage testing of microwave imaging devices. If required for a study, a more complex and more anatomically accurate phantom could be fabricated, by direct extension of the principles described here.

To achieve an accurate anatomical shape, 3D printed moulds of an actual human brain and head were produced using STL files from [18] and [19]. The former was created from a reverse engineered polygon mesh while the latter was derived from MRI data. These were printed with an Ultimaker 2+ Extended 3D printer. The 3D printed head mould was too fragile to withstand the process of fabrication and so a counter mould made of polyurethane was fabricated using the 3D printed mould. This was achieved by pouring polyurethane into a polystyrene box before placing the head mould inside until the polyurethane set. This counter mould is shown in Fig. 3 along with the 3D printed brain mould.

The scalp-cortex distance data at various positions around the head [29] was used to ensure the brain mould was positioned correctly, with respect to the surface of the head counter mould — approximately 15 mm on the top of the head and 11 mm on the lateral, anterior and posterior sides. The outer layer is

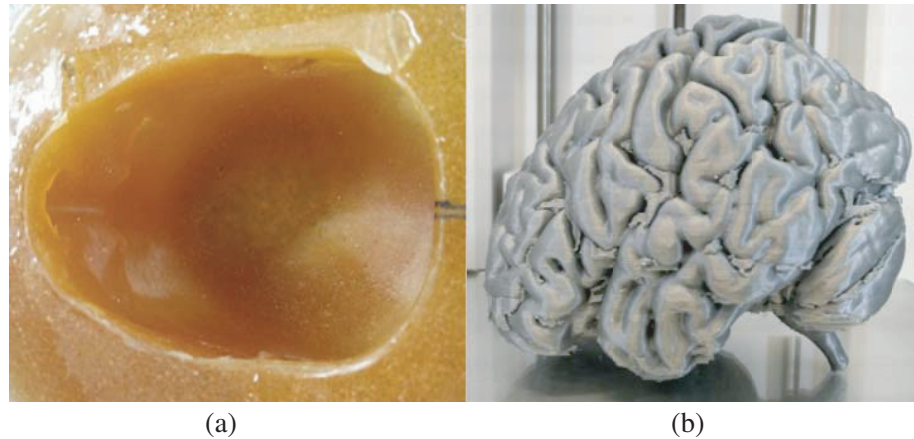


Figure 3. (a) Head counter mould made from polyurethane and (b) 3D printed brain mould for head phantom fabrication.



Figure 4. (a) External layer poured and laid inside the head counter mould with the brain mould positioned inside, a wire is attached to the brain mould to aid in its removal once the external layer is set. (b) Once set, the brain mould is removed intact to leave the outer layer with an impression of the exterior surface of the brain on its inner side.

constructed from the crown of the head down as far as the level of the philtrum. This level aligns with the base of the brain and the top of the spinal cord [30]. Further, the skull ends and the soft tissues of the head begin to close in around the base of the brain here [30]. Had the model continued (and narrowed) below this point, it would render removal of the brain mould impossible. As the objective of this phantom is to model the brain and surrounding tissues, including the skull, it is unnecessary to develop the phantom beyond this level.

Figure 4 shows the external tissue layer inside the head counter mould with the brain mould embedded in the correct position. A wire attached to the brain mould aids its removal once the external layer is set. Once the brain mould is removed the outer layer is complete and has an impression of the external surface of the brain on its inner side, as displayed in Fig. 4.

Two 3D printed cylindrical plugs, of 25 mm diameter and penetrating to within 5 mm of the start of the external layer, were then securely placed symmetrically on the left and right sides of the sagittal plane through the cavity. The flat surface of the cylindrical plugs meant they could not be put in direct contact with the irregularly curved surface of the inner surface of the external layer without the risk of air-gaps when filled with phantom plugs later. The 5 mm of brain material is enough to ensure a flat surface and yet be near enough to replicate lesions at or near the brain surface. The plug diameter

of 25 mm allows replication of lesions of various shapes and sizes, with this as a limiting dimension. Intracerebral haemorrhages (ICH) for example often adopt a ellipsoid topology [31] with the median ICH volume being about 17 ml in the early stage [32]. A sphere, being a simplification of an ellipsoid, of diameter 25 mm fabricated from blood mimicking TMM would replicate a haemorrhage of volume 8 ml, while an ellipsoid 20 mm \times 20 mm \times 10 mm would represent a volume of approximately 17 ml. Hence, a 25 mm plug size allows testing of haemorrhages which cover the real world expected range.

A piece of narrow rubber tubing, in the shape of a smooth arc and of diameter 4 mm with a 3 mm lumen was used to create a simplified model circulatory loop. The principal arterial structure serving the brain, the Circle of Willis, and the major vessels distal and proximal to it such as the basilar artery, internal carotid artery and the cerebral arteries are all of similar vessel dimensions [33]. The tubing was placed posterior to the plugs in a symmetrical loop across the midline with the apex half way into the brain cavity depth.

Next, the brain TMM mixture was packed into the cavity and allowed to set, resulting in the brain layer with two cylindrical hollows once the plugs were removed. The ends of the rubber tubing were also visible and accessible. These hollows are filled with plugs, containing only brain TMM, or brain TMM with discrete lesions like haemorrhages made from blood TMM. The tubing allows replication of blood flow by passing a fluid through it; for instance, physiological saline.

The cylindrical phantom plugs are fabricated using a corresponding cylindrical mould, produced in two halves with fixtures to hold the halves together as seen in Fig. 5. These plugs are inserted into the hollows, similar to the methodology described in [14]. Plugs created exclusively from the brain mimicking TMM were used to model a normal brain when inserted, while various phantom bleeds were fabricated using the blood mimicking TMM. The bleeds were of known, controlled size and shape, were always small enough to fit in the cylindrical hollows, and when set could be placed into the cylindrical mould with brain mimicking TMM surrounding and encasing them. Using these techniques, plugs with pathologic haemorrhagic lesions could be placed in the brain phantom alongside normal brain plugs or other haemorrhagic plugs. Examples of these haemorrhagic phantom lesions and tissue plugs are shown in Fig. 6.

Finally, the complete head phantom was removed from the counter mould. The fabricated head phantom supporting its own weight upright, and inverted to show the plugs and tubing, is shown in Fig. 7. Due to the plugs protruding from the base along with the ends of the tubing, a stand was fabricated to support the phantom along its edges, but leave the base exposed and elevated.



Figure 5. Cylindrical plugs (1) used to make cylindrical cavities in the brain layer and cylindrical phantom plug mould equipment (2, 3). To create a plug, the phantom material is packed into the two halves (2), which are then joined and held together by the supports (3) shown which are placed on the top and bottom of the joined halves until the material sets.



Figure 6. Haemorrhagic phantom lesions (bottom) are shown alongside an example of a completed cylindrical phantom tissue plug (top). These plugs are either made wholly of the brain mimicking TMM or have a haemorrhagic phantom lesion embedded in them at a known location. Haemorrhagic phantom lesions can be of any size or shape as long as they fit within the dimensions of the cylindrical plug. These plugs are fitted into the cavities in the brain part of the head phantom to complete it.



Figure 7. Photograph of the fabricated dielectrically and anatomically realistic head phantom. The phantom contains two 25 mm diameter cylindrical hollows bilaterally located across the sagittal plane along with a symmetrically placed circulatory loop across the midline. The head phantom is shown upright ((a), (b) and (d)) and inverted ((c)). The inverted view shows the two cylindrical cavities, which can be filled with phantom plugs, as well as the entry and exit points of the rubber tubing used to create the circulatory loop. The loop forms an arc with the apex reaching approximately half way into the brain cavity.

3.2. Results & Discussion

Fabrication of the phantom is as important as TMM development in order to translate the dielectrically and mechanically stable building blocks provided by the TMM mixtures into an anatomically realistic, mechanically and dielectrically stable model of the body-region of interest, thus providing an accurate test platform for MWD studies. As such, due diligence in the fabrication process is vital. Some of the challenges and notable points encountered in the building of the overall head phantom are given below.

The head counter mould had an incision made in the sagittal plane to a level half way down the mould. This incision allowed both sides be pulled open when inserting and removing the brain mould and to allow ease of access when adding the first layer of outer TMM material. A Perspex enclosure around the cuboid counter mould ensured no deformation of the counter mould could occur.

The 3D moulds of the head and brain were challenging to print. 3D printers perform well with simple geometric objects, but objects with intricate and complex contours such as the brain with its associated sulci and gyri can result in the printer mal-functioning. Ultimately, the moulds were printed at low speed with successful prints taking 2–3 days to complete. This is only a limitation in the first instance since once the 3D brain mould is printed, it is reusable for subsequent phantoms.

The TMMs were relatively easy to prepare for each layer. In particular, the 3% w/w (mass percentage) isopropanol used in the TMM mixtures with a large percentage of graphite and carbon black (brain TMM and blood TMM) significantly made the mixing process easier. Other candidate mixtures with similar proportions of graphite and carbon black, but less or no acetone or isopropanol were difficult to mix homogenously and tended to have unmixed granules left over, similar to the findings in [8]. It was determined that the same percentage of isopropanol added to a mixture would result in higher conductivity, and similar permittivity, compared to those using acetone. This increase in conductivity was thought to be a consequence of the dispersion effect of alcohols on graphite and carbon black causing more conductive pathways [28]. This effect was especially significant for mixtures involving higher percentages of graphite and carbon black, such as the candidate blood and brain TMMs. Isopropanol was needed to ensure realistic conductivity to emulate relatively high conductivity tissues, such as blood, as acetone was found not to produce high enough values for such tissues. However, samples made with isopropanol were somewhat more friable than those without but despite this, the TMM's mechanical robustness was still more than adequate to work with.

The TMMs, once made, were easy to mould and shape and were mechanically and dielectrically stable. The overall phantom was also anatomically realistic with the cylindrical plugs fitting smoothly and firmly. The phantom was capable of supporting its own weight and could be rested upright on a stand. To replicate blood flow, and hence render the test scenario more realistic, fluid (we propose saline) should be pumped through the embedded tubing. Overall, the developed head phantom incorporates realistic anatomy, physiology, and dielectric properties, and as such will provide an excellent test platform for MWD technologies.

4. CONCLUSION

Tissue-mimicking materials based on graphite, carbon black, polyurethane, and acetone or isopropanol have been shown in this study to be easily fabricated and capable of spanning a wide range of relative permittivity and conductivity values by adjusting the proportion of ingredients. Hence any biological tissue, or aggregate tissue, can be emulated using a suitable tissue mimicking material (TMM) mixture. This finding is demonstrated here, as, for the first time, tissue mimicking materials for tissues of the head are developed using this material set. Further, the novel use of isopropanol to increase conductivity to realistic levels has been proposed.

The TMMs are easily mouldable, relatively inexpensive compared to other solid TMMs, and mechanically and dielectrically stable over time. The resultant phantoms created from the TMMs share these attributes.

3D printed moulds produced from anatomically precise STL files enable the reproduction of realistic structures that can be employed to fabricate multi-layered phantoms. The head phantom created for this study is an example of this concept, comprising of two layers — an outer aggregate layer modelling the tissues of the head external to the brain (skin, skull cortical bone, skull cancellous bone, meninges and CSF) and an inner aggregate layer, modelling the grey matter, white matter and CSF of the brain.

Pathology is modelled and adjusted through the use of cylindrical plugs. In this paper a blood TMM replicating haemorrhage is demonstrated but the concept can be extended to include tumours or any other suitable pathology, which features a distinct lesion of a particular tissue or tissue aggregate. Finally, for the first time, a simplified physical model of circulation is incorporated into the head phantom in order to mimic blood flow and model physiology. This improves the realism of the test phantom. In the future, steps may be taken toward making a phantom that further improves the replication of the human head, if desired for a given experimental investigation. For instance, one could add more tissue types and layers, add more tubes for a more anatomically accurate circulatory system, and add airways for an air mimicking TMM for nasal cavity.

In conclusion, this novel, realistic and modifiable head phantom will provide a valuable tool for microwave diagnostic studies.

ACKNOWLEDGMENT

The research leading to these results has received funding from the European Research Council under the European Union's Horizon 2020 Programme/ ERC Grant Agreement BioElecPro n.637780, Science Foundation Ireland (SFI) Grant #15/ERCS/3276, and the Hardiman Research Scholarship, NUIG.

REFERENCES

1. Bath, P. M. W., "ABC of arterial and venous disease: Acute stroke," *BMJ*, Vol. 320, No. 7239, 920–923, Apr. 2000.
2. Lee, B. and A. Newberg, "Neuroimaging in traumatic brain imaging," *NeuroRX*, Vol. 2, No. 2, 372–383, Apr. 2005.
3. Birenbaum, D., L. W. Bancroft, and G. J. Felsberg, "Imaging in acute stroke," *West. J. Emerg. Med.*, Vol. 12, No. 1, 67–76, Feb. 2011.
4. Semenov, S., "Microwave tomography: Review of the progress towards clinical applications," *Philos. Trans. A. Math. Phys. Eng. Sci.*, Vol. 367, 3021–3042, 2009.
5. Garrett, J. and E. Fear, "A new breast phantom with a durable skin layer for microwave breast imaging," *IEEE Trans. Antennas Propag.*, Vol. 63, No. 4, 1693–1700, 2015.
6. Mobashsher, A. T. and A. M. Abbosh, "Artificial human phantoms: Human proxy in testing microwave apparatuses that have electromagnetic interaction with the human body," *IEEE Microw. Mag.*, Vol. 16, No. 6, 42–62, 2015.
7. Fear, E. C., P. M. Meaney, and M. Stuchly, "Microwaves for breast cancer detection?," *IEEE Potentials*, Vol. 22, No. 1, 12–18, Feb. 2003.
8. Garrett, J. and E. Fear, "Stable and flexible materials to mimic the dielectric properties of human soft tissues," *IEEE Antennas Wirel. Propag. Lett.*, Vol. 13, 599–602, 2014.
9. Peyman, A., A. A. Rezazadeh, and C. Gabriel, "Changes in the dielectric properties of rat tissue as a function of age at microwave frequencies," *Phys. Med. Biol.*, Vol. 46, No. 6, 1617–1629, Jun. 2001.
10. Kobayashi, T., T. Nojima, K. Yamada, and S. Uebayashi, "Dry phantom composed of ceramics and its application to SAR estimation," *IEEE Trans. Microw. Theory Tech.*, Vol. 41, No. 1, 136–140, 1993.
11. Watanabe, S.-I., H. Taki, T. Nojima, and O. Fujiwara, "Characteristics of the SAR distributions in a head exposed to electromagnetic fields radiated by a hand-held portable radio," *IEEE Trans. Microw. Theory Tech.*, Vol. 44, No. 10, 1874–1883, 1996.
12. Mobashsher, A. T. and A. M. Abbosh, "Three-dimensional human head phantom with realistic electrical properties and anatomy," *IEEE Antennas Wirel. Propag. Lett.*, Vol. 13, 1401–1404, 2014.
13. Otterskog, M., N. Petrovic, and P. O. Risman, "A multi-layered head phantom for microwave investigations of brain hemorrhages," *2016 IEEE Conference on Antenna Measurements & Applications (CAMA)*, 1–3, 2016.
14. Santorelli, A., O. Laforest, E. Porter, and M. Popovi, "Image classification for a time-domain

- microwave radar system: Experiments with stable modular breast phantoms,” *European Conference on Antennas and Propagation (EuCAP)*, 2015.
15. Gabriel, C., S. Gabriel, and E. Corthout, “The dielectric properties of biological tissues: I. Literature survey,” *Phys. Med. Biol.*, Vol. 41, No. 11, 2231–49, 1996.
 16. Gabriel, S., R. W. Lau, and C. Gabriel, “The dielectric properties of biological tissues: III. Parametric models for the dielectric spectrum of tissues,” *Phys. Med. Biol.*, Vol. 41, No. 11, 2271–93, 1996.
 17. Hasgall, P., F. DiGennaro, C. Baumgartner, E. Neufeld, M. Gosselin, D. Payne, A. Klingenböck, and N. Kuster, “IT’IS Database for thermal and electromagnetic parameters of biological tissues,” 2015, [Online], Available: www.itis.ethz.ch/database, [Accessed: 25-Nov-2016].
 18. Grozny, “Thingiverse — Human Head,” [Online], Available: <http://www.thingiverse.com/thing:172348>, [Accessed: 15-Feb-2017].
 19. Dilmen, N., “NIH 3D print exchange — Brain MRI,” [Online], Available: <https://3dprint.nih.gov/discover/3DPX-002739>, [Accessed: 15-Feb-2017].
 20. Foster, K. R., J. L. Schepps, R. D. Stoy, and H. P. Schwan, “Dielectric properties of brain tissue between 0.01 and 10 GHz,” *Phys. Med. Biol.*, Vol. 24, No. 6, 1177–1187, 1979.
 21. Schmid, G., G. Neubauer, and P. R. Mazal, “Dielectric properties of human brain tissue measured less than 10 h postmortem at frequencies from 800 to 2450 MHz,” *Bioelectromagnetics*, Vol. 24, No. 6, 423–430, 2003.
 22. Gabriel, C. and A. Peyman, “Dielectric measurement: Error analysis and assessment of uncertainty,” *Phys. Med. Biol.*, Vol. 51, No. 23, 6033–6046, 2006.
 23. Pethig, R., “Dielectric properties of body tissues,” *Clin. Phys. Physiol. Meas.*, Vol. 8 Suppl A, 5–12, 1987.
 24. Hyttinen, J., P. Kauppinen, T. Koobi, and J. Malmivuo, “Importance of the tissue conductivity values in modelling the thorax as a volume conductor,” *19th Annu. Int. Conf. IEEE Eng. Med. Biol. Soc.*, Vol. 19, No. C, 2082–2085, 1997.
 25. Gabriel, C., “Dielectric properties of biological tissue: Variation with age,” *Bioelectromagnetics*, Vol. 26, No. Suppl. 7, 12–18, 2005.
 26. Lüders, E., H. Steinmetz, and L. Jäncke, “Brain size and grey matter volume in the healthy human brain,” *Neuroreport*, Vol. 13, No. 17, 2371–4, 2002.
 27. Makris, N., L. Angelone, S. Tulloch, S. Sorg, J. Kaiser, D. Kennedy, and G. Bonmassar, *Absorption Rate Mapping*, Vol. 46, No. 12, 1239–1251, 2010.
 28. Kim, D.-Y., R. Jung, H.-S. Kim, and H.-J. Jin, “Electrically conductive polymeric nanocomposites prepared in alcohol dispersion of multiwalled carbon nanotubes,” *Mol. Cryst. Liq. Cryst.*, Vol. 491, No. 1, 255–263, Sep. 2008.
 29. Stokes, M. G., C. D. Chambers, I. C. Gould, T. R. Henderson, N. E. Janko, N. B. Allen, J. B. Mattingley, A. T. Barker, M. Dervinis, F. Verbruggen, L. Maizey, R. C. Adams, R. Henderson, and B. Jason, “Simple metric for scaling motor threshold based on scalp-cortex distance: Application to studies using transcranial magnetic stimulation simple metric for scaling motor threshold based on scalp-cortex distance: Application to studies using transcranial,” *J. Neurophysiol.*, Vol. 94, No. 6, 4520–7, 2005.
 30. Standring, S., *Gray’s Anatomy: The Anatomical Basis of Clinical Practice*, 40th Edition, Elsevier, 2009.
 31. Sims, J. R., L. R. Gharai, P. W. Schaefer, M. Vangel, E. S. Rosenthal, M. H. Lev, and L. H. Schwamm, “ABC/2 for rapid clinical estimate of infarct, perfusion, and mismatch volumes,” *Neurology*, Vol. 72, No. 24, 2104–2110, 2009.
 32. Mobashsher, A. T., K. S. Bialkowski, A. M. Abbosh, and S. Crozier, “Design and experimental evaluation of a non-invasive microwave head imaging system for intracranial haemorrhage detection,” *PLoS One*, Vol. 11, No. 4, Apr. 2016.
 33. Curry, R. A. and B. B. Tempkin, *Sonography — E-Book: Introduction to Normal Structure and Function*, 3rd Edition, Saunders, 2014.